frontiers | Frontiers in Cell and Developmental Biology

A versatile enhanced freeze-substitution protocol for volume electron microscopy

Sébastien Bélanger[1], Heather Berensmann[2,3],
Valentina Baena[2,3], Keith Duncan[1], Blake C. Meyers[1,4],
Kedar Narayan[2,3] and Kirk J. Czymmek[1,5]*

[1]Donald Danforth Plant Science Center, Saint Louis, MO, United States, [2]Center for Molecular Microscopy, Center for Cancer Research, National Cancer Institute, National Institutes of Health, Bethesda, MD, United States, [3]Cancer Research Technology Program, Frederick National Laboratory for Cancer Research, Frederick, MD, United States, [4]Division of Plant Science and Technology, University of Missouri–Columbia, Columbia, MO, United States, [5]Advanced Bioimaging Laboratory, Donald Danforth Plant Science Center, Saint Louis, MO, United States

Volume electron microscopy, a powerful approach to generate large three-dimensional cell and tissue volumes at electron microscopy resolutions, is rapidly becoming a routine tool for understanding fundamental and applied biological questions. One of the enabling factors for its adoption has been the development of conventional fixation protocols with improved heavy metal staining. However, freeze-substitution with organic solvent-based fixation and staining has not realized the same level of benefit. Here, we report a straightforward approach including osmium tetroxide, acetone and up to 3% water substitution fluid (compatible with traditional or fast freeze-substitution protocols), warm-up and transition from organic solvent to aqueous 2% osmium tetroxide. Once fully hydrated, samples were processed in aqueous based potassium ferrocyanide, thiocarbohydrazide, osmium tetroxide, uranyl acetate and lead acetate before resin infiltration and polymerization. We observed a consistent and substantial increase in heavy metal staining across diverse and difficult-to-fix test organisms and tissue types, including plant tissues (*Hordeum vulgare*), nematode (*Caenorhabditis elegans*) and yeast (*Saccharomyces cerevisiae*). Our approach opens new possibilities to combine the benefits of cryo-preservation with enhanced contrast for volume electron microscopy in diverse organisms.

Introduction

A number of three-dimensional (3D) approaches have been developed that enable intermediate and high-resolution imaging of cells and tissues, each with their own merits and limitations (Watanabe et al., 2014; Collman et al., 2015; Mahamid et al., 2015; Sydor et al., 2015; Hoffman et al., 2020; Otegui, 2020; Wu et al., 2020). Volume electron microscopy (vEM), is particularly suitable when the collection of nanometer scale data from relatively large samples (100–1000 s of um³) and 100–1000 s of serial sections of resin embedded specimen is required (Titze and Genoud, 2016). This can be achieved by generating consecutive sections arranged in arrays on a substrate, termed array tomography (AT) (Mendenhall, Kuwajima and Harris, 2017; Smith, 2018) or by the serial removal of a thin surface layer and imaging the exposed block-face (Narayan et al., 2014; Guérin et al., 2019; Lippens et al., 2019). With AT, sections cut into ribbons and attached to a surface, post-stained with heavy metals and rendered conductive, allows many traditional fixation/staining protocols as well as affinity probe labeling for correlative microscopy. For serial block-face imaging, an in-chamber ultramicrotome repeatedly shaves the resin surface using a diamond knife and is known as serial block-face scanning electron microscopy (SBF-SEM) (Denk and Horstmann, 2004). Alternatively, a focused ion beam "mills" the resin surface, termed focused ion beam scanning electron microscopy (FIB-SEM) (Narayan and Subramaniam, 2015). Both SBF-SEM or FIB-SEM rely on heavy metal-induced backscatter electrons to generate image contrast, and all metal staining steps of the bulk sample must be performed "en bloc," prior to resin infiltration and polymerization. Furthermore, image quality (signal-to-noise), structure, resolution and sample conductivity are highly dependent upon the levels of metal staining of the sample constituents. Arguably, one of the significant technical advances that helped propel the adoption of SBF-SEM for volume electron microscopy (vEM) studies was the amplification of metal staining via osmium-thiocarbohydrazide-osmium (OTO), often with potassium ferrocyanide, lead and uranium salts (Deerinck et al., 2018).

Conventional fixative protocols at ambient temperatures often result in subcellular changes due to fixation artifacts. Immobilizing cellular structures within milliseconds, using freezing, offers optimal morphological preservation of many cellular structures, preserving them in their near-native state (Gilkey and Staehelin, 1986). While freeze-substitution fixation with organic solvent-based staining protocols provides remarkable cellular renditions via post-stained resin sections and transmission electron microscopy (TEM), it often results in very low contrast in certain cell structures (i.e., membranes and cell walls) and overall intense metal staining of traditional freeze-substitution preparations comparable to aqueous OTO remains elusive. Poor membrane visibility often can be addressed by the addition of up to 5% water in the freeze-substitution solution (Buser and Walther, 2008), or other substitution fluid modifications (Guo et al., 2020). SBF-SEM in particular is more sensitive to reduced sample conductivity when samples have large non-cellular voids (i.e., vacuoles and/or air spaces). The use of organic solvent-based OTO and/or en bloc lead and uranium salts have indeed helped improved contrast and signal-to-noise for vEM (Tsang et al., 2018; Czymmek et al., 2020), including increased chamber pressure and local gas injection strategies (Deerinck et al., 2018) and the inclusion of conductive resins (Nguyen et al., 2016) to suppress charge. Despite these improvements, the level of metalization, compared with aqueous OTO protocol counterparts, still limits a number of SBF-SEM and FIB-SEM experiments where improved resolution (x-y, z), speed of acquisition and sample tolerance to beam dosage are required.

To address this, we developed an approach that builds on the work of others using rehydration strategies with HPF freeze-substituted samples (Ripper, Schwarz and Stierhof, 2008; Tsang et al., 2018). We transitioned from organic solvent to an aqueous osmium tetroxide (OsO_4) solution upon warm-up, and followed this with an aqueous solvent-based metal staining protocol designed to improve uniformity of OTO preparations in larger samples (Hua, Laserstein and Helmstaedter, 2015; Genoud et al., 2018; Duncan et al., 2022). Our strategy was based upon the notion that the reduced solubility and staining capacity of metal stain components in polar organic vs. aqueous solvents for cryo-preparations could be surmounted and further improved. We developed and evaluated our Freeze-Substitution and aqueous OTO protocol (FSaqOTO) using several diverse and challenging plant, animal, and yeast test samples. We included side-by-side aqueous vs. organic FS comparisons that demonstrated substantial signal improvement and distinctive staining patterns of certain cell structures with the FSaqOTO protocol. Additionally, our FSaqOTO protocol was versatile; it is compatible with manual, automated and quick-freeze substitution warm-up regimes. While not a panacea, our current FSaqOTO protocol is likely suitable for many organisms and studies for which cryo-preservation is the gold-standard approach, but aqueous enhanced metalization is required to substantially improve signal-to-noise, throughput, and enhanced staining of certain cell structures for intermediate resolution vEM structural studies.

Materials and methods

High-pressure freezing approach for tested specimen

All specimens were frozen in a Leica EM ICE High-Pressure Freezer (Leica Microsystems, Inc., Buffalo Grove, IL, United States) as follows:
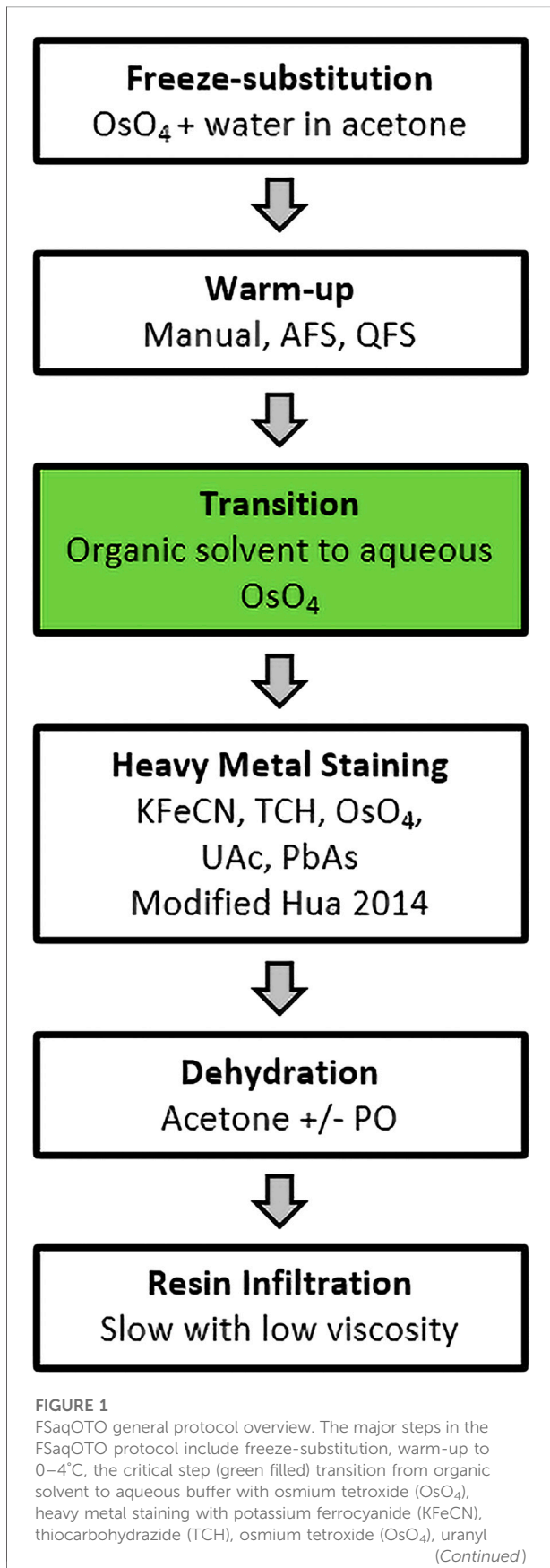
Plant: Root tips and anthers (0.8 and 1.5 mm) were excised via scalpel from barley (*Hordeum vulgare ssp. vulgare*) and placed in 3 mm gold-coated copper planchettes (one Type A, Cat # 16770152 and one Type B, Cat# 16770152, cavity space 400 um) with 50 mM sucrose in 75 mM PIPES buffer (pH 7.2) as a space filler and high-pressure frozen.

Nematode: *Caenorhabditis elegans* were maintained on MYOB agar plates seeded with *E. coli* OP50 bacteria and prepared for high pressure freezing as described previously (Rahman et al., 2021). Briefly, nematodes were collected in cellulose capillary tubes (Leica catalog number 16706869) and placed in 3 mm gold-coated copper planchettes (Type A and B, cavity space 300 um) with 20% dextran as a space filler and high-pressure frozen.

Yeast: *Saccharomyces cerevisiae* (strain BJ5494) was grown in YEPD medium to mid-log phase in a shaker flask at 60 RPM and 32°C, harvested by gentle centrifugation on a tabletop device to create a paste and placed in 3 mm gold-coated copper planchettes (Type A and B, cavity space 100 um) without additional space filler and high-pressure frozen.

Freeze-substitution and rehydration

High-pressure frozen samples were processed for freeze-substitution, heavy metal stained and resin infiltrated according to the general protocol overview shown in Figure 1. The overall approach was robust and allowed variations in substitution fluid, resin formulation and warm-up strategy.

HPF frozen plant materials were placed in mPrep/s capsules (Microscopy Innovations, Cat # 2250) without mPrep screens and held in mPrep CPD Holder (Microscopy Innovations, Cat # 2250) that was then placed in a 50 ml PTFE beaker (EMS Diasum, Cat# 60942) containing LN_2 frozen substitution fluid (2% OsO_4 in acetone with 3% water) and subsequently moved to −85°C for 3–4 days (Supplementary Data S1). Specifically, the mPrep capsule/ CPD holder/PTFE assembly and pre-chilled substitution fluids were prepared by placing in adjacent Styrofoam containers with dry ice in a chemical fumehood. Next, the substitution fluid was added to the PTFE assembly until the fluid level was flush with the top of the mPrep CPD holder. The substitution fluid filled PTFE assembly was then carefully transferred (with forceps) and slowly lowered to the bottom of a shallow Styrofoam container with a few inches of LN_2 (be sure LN_2 level is maintained ~1 cm below top of PTFE container) until the solution was frozen. Aluminum planchettes and substitution containers should be avoided as the heavy metal

staining steps react with aluminum (i.e. TCH) turning the solution black and subsequent use of aluminum containers with this chemistry resulted in their failure (leakiness). Samples were then transferred step-wise and held at −55°C and −20°C for 3 h each and moved to 4°C for 1 h and room temperature for 1 h. At 4°C, a second mPrep/s capsule was inserted into each initial mPrep/s capsule to entrap and immerse the small specimen during subsequent aqueous-based processing steps. This prevented specimen loss and ensured the buoyant plant specimens were completely submerged in all reagents, thus minimizing uneven staining and/ or inadequate reagent exchange. The critical organic solvent to aqueous transition step was performed at 4°C, where samples were rehydrated (20 min each step) in 1% OsO_4 using the following graded series of water:acetone 1:4, 1:1, 4:1 and finally moved to room temperature in 1% OsO_4 in 0.1 M sodium cacodylate buffer (pH 7.4) for 1 h.

For protocol comparison purposes, freeze-substitution was applied using a traditional Automated Freeze-substitution System (AFS, Leica Microsystems) (Rahman et al., 2021) without FSAqOTO, and Quick Freeze-Substitution (QFS) (Mcdonald and Webb, 2011) with our enhanced aqueous metalization approach to the model organisms *S. cerevisiae* and *C. elegans*. With AFS, the freeze-substitution cocktail was 1% OsO_4 and 1% glutaraldehyde in 1% water in acetone. 1 ml of freeze-substitution cocktail was placed in each cryovial and frozen under liquid nitrogen. The planchettes holding the frozen samples were transferred under liquid nitrogen vapors into the cryovials containing the frozen freeze-substitution cocktail. The cryovials were then capped and placed in the Leica AFS 2 chamber (set to −90°C) in aluminum containers with pre-cooled ethanol. The AFS program was run as follows: −90°C for 48 h, −90°C to −60°C for 6 h (5°C/h), −60°C for 2 h, −60°C to −20°C for 8 h (5°C/h), −20°C for 2 h, -20–0°C for 4 h (5°C/h). After freeze-substitution, the samples were rinsed with pre-cooled (to 0°C) acetone 3 times for 10 min each. After the third wash, samples were removed from the AFS chamber and allowed to reach room temperature. Samples were placed in 1% uranyl acetate in acetone for 1 h at room temperature followed by 3 acetone washes for 10 min each before proceeding to resin infiltration (see below).

In addition to AFS, we applied a Quick Freeze-Substitution aqueous OTO protocol for both the *S. cerevisiae* and *C. elegans* samples. Briefly, after high pressure freezing in an Leica EM ICE, the FSaqOTO protocol was performed largely following Rahman (Rahman et al., 2021) and McDonald (McDonald, 2014), but with slight changes to the actual freeze-substitution solvent and stain mixtures (referred to as SubMix). For *S. cerevisiae* samples, a SubMix of 1% w/v OsO_4 and 1% w/v UAc dissolved in 90% acetone +5% methanol +5% water was prepared. For *C. elegans*, a SubMix of 1% w/v OsO_4 dissolved in 97% acetone +3% water was prepared. Briefly, 1 ml of these SubMixes were aliquoted into cryovials and inserted into a metal block, which was laid on its side in an ice bucket. The bucket was filled with liquid nitrogen,

and after the SubMixes were frozen, the high-pressure frozen planchettes with the samples were quickly transferred to the cryovials. The liquid nitrogen was poured out and dry ice packed in (for a detailed step-by-step protocol with images and catalog numbers, please see Rahman (Rahman et al., 2021)). The ice bucket was put on a rotary shaker set at 60 rpm, and rotated for 3 h with the lid on, 1 h with the dry ice poured out but the lid still on, and finally with the lid off until the temperature reached 0°C, typically 1 h. At this point, rather than continue with the freeze-substitution in the mostly anhydrous SubMix, the metal block was surrounded by ice packs to maintain temperatures around 0°C. Then, the SubMix was carefully replaced with previously made and cooled dilutions of the SubMix. Thus, the samples were incubated with 1 ml pre-chilled solutions of SubMix:water ratios of 3:1, 1:1, 1:3 each for 20 min, with the shaker still set at 60 rpm. Finally, the solution was replaced with 1% OsO_4 in 0.1 M sodium cacodylate buffer and allowed to equilibrate to room temperature for 1 h. After this step, the Hua heavy metal staining protocol (Hua et al., 2015) was largely followed, except we used PolyBed resin, hard formulation (resin infiltration details below).

Heavy metal staining

We subsequently performed a modified version of the OTO staining method developed by Hua et al. (2015) for sample metallization of large mouse brain specimens. We removed the OsO_4 solution and placed directly into 2.5% potassium ferrocyanide (#9387-100G; Sigma-Aldrich, St Louis, MO, United States) in 0.1 M sodium cacodylate at pH 7.4 for 90 min at room temperature. We then washed samples (2 × 30 min in water) and transferred samples into 1% TCH (#21900; EMS, Hatfield, PA, United States) in water for 45 min at 40°C. We washed samples (2 × 30 min in water) at room temperature again and transferred samples into 2% OsO_4 in water for 90 min at room temperature. We washed samples (2 × 30 min in water) and transferred samples in an unbuffered 1% aqueous uranyl acetate at 4°C, overnight. The samples in 1% aqueous uranyl acetate were then moved to 50°C for 2 h and washed (2 × 30 min in water) and transferred to lead aspartate in water for 2 h at 50°C. The lead aspartate was prepared with 0.04 g L-aspartic acid (#a9256; Sigma-Aldrich, St Louis, MO, United States) and 0.066 g lead nitrate (#203580-10G; Sigma-Aldrich, St Louis, MO, United States) in 10 ml water and the pH was adjusted to 5.5. Finally, samples were washed (2 × 30 min in water) at room temperature.

Sample dehydration, infiltration and embedding

For *H. vulgare,* prior to infiltration and sample embedment, we performed a graded dehydration series of 30, 50, 70, 80, 90, 100 and

100% acetone at 4°C for 30 min each. The dehydrated samples were exchanged 2X in 100% propylene oxide (#20401; EMS, Hatfield, PA, United States) for 30 min each. Samples were then resin infiltrated with a graded series of 25, 50, 75 and 100% Quetol resin (hard formulation) in propylene oxide without DMP-30 (#14640; EMS, Hatfield, PA, United States) at room temperature for 24 h each step on a rocking platform to enhance resin infiltration. Please note that with our tested plant samples, improved consistency in block quality and uniformity was achieved with use of propylene oxide. However, due to its toxicity, use of propylene oxide is sample dependent and can be omitted and replaced with acetone for resin infiltration steps for less challenging samples. All samples were removed from the mPrep/s capsules at the 50% acetone graded series step and then processed in glass vials for remaining steps. Subsequently, two overnight 100% resin exchanges were made with DMP-30. Finally, samples were embedded in freshly made 100% Quetol using flat embedding molds (#70900; EMS, Hatfield, PA, United States).

For *C. elegans* and *S. cerevisiae*, resin infiltration (using Polybed 812, DDSA, NMA, Polysciences, Inc. BDMA, Electron Microscopy Sciences) was done at room temperature as follows: *C. elegans* - 1:3 resin:acetone for 2 h, 1:1 resin:acetone for 2 h, 3:1 resin:acetone overnight, 100% resin for 5 h. *S. cerevisiae* - 1:3 resin:acetone for 2 h, 1:1 resin:acetone overnight, 3:1 resin:acetone for 3 h, 100% resin overnight. Samples were embedded in molds with fresh resin and polymerized in a 60°C oven for 2 days. The resin embedded samples were trimmed and sectioned to expose the sample on the section face, after which the resin block was cut, mounted on a stub, gold coated and introduced into a CrossBeam550 (ZEISS, Oberkochen, Germany) for high-resolution FIB milling and SEM imaging.

All major steps in sample preparation conditions from fixation to resin are detailed in Supplementary Data S2.

SBF-SEM, FIB-SEM, STEM and TEM image acquisition

Embedded tissues were mounted on a 1.4 mm standard Gatan flat pin using silver conductive epoxy (Chemtronics, CW2400, Kennesaw, GA, United States), trimmed and sectioned using the Leica Ultracut UCT (Leica Microsystems Inc., Buffalo Grove, IL, United States). Due to the extremely opaque nature of the metalized samples prepared in this way, sample quality was assessed with any of the following approaches: whole block imaging by X-ray microscopy or unstained semi thick sections (350 nm) via light microscopy. For TEM ultrathin sections (~70 nm) were imaged at 80 kV using a Hitachi H7650 equipped with an Advanced Microscopy Techniques model XR41 digital camera with 2048 × 2048 pixel resolution and 2 nm pixel size. For SBF-SEM, pins with resin blocks were sputter coated with an ~50 nm layer of gold/palladium. Then, over 1000 sequential images at a 10 k x 10 k pixel

resolution and 5 nm x-y, 50 nm z-step size were collected on a ZEISS GeminiSEM 300 SEM at 5 kV (current of 1 pA, and 3 µs dwell time) using a Gatan 3-View® 2XP and local N_2 gas injection via a Focal Charge Compensation (FCC) needle set between 10 and 35%.

FIB-SEM imaging was performed on a Zeiss CrossBeam 550, using the ATLAS3D module, as previously described (Narayan et al., 2014). After the specimen were coated with a patterned platinum and carbon pad, images were acquired at either 3 or 5 nm pixel sampling and 4 µs total pixel dwell time, with electron beam parameters of 1.5 kV and 1 nA and the grid voltage at the in-column backscatter detector set at 900 V. The FIB-SEM was operated at 30 kV, 1.5 µA, with a step size of either 9 nm or 15 nm, respectively. The resulting image stacks were registered, contrast inverted and binned to yield isotropic image volumes. STEM images were acquired on a Zeiss GeminiSEM 450 equipped with a STEM detector and operated at 30 kV. Images were acquired at 3, 10, or 15 nm x-y pixel sampling.

All manuscript figures and corresponding imaging conditions are detailed in Supplementary Data S3.

Image processing, segmentation, reconstruction and visualization of specimen volumes

Three-dimensional volumes of selected specimens were generated using the Object Research Solutions (ORS, Montréal, Canada) Dragonfly Version 2020.2 Build 941. For segmentation and deep learning, an ~180 image 10 k x10 k subset of the full stack was processed using the ORS Segmentation Wizard. Three slices were fully trained representing eight target features. A three-level Sensor 3D deep learning model with a patch size of 64 (Supplementary Data S4) yielded good results for our aqueous OTO freeze-substitution protocol for plant cell walls, mitochondria, Golgi and vesicles in 3D surface renderings (Figure 1E).

Results

FSaqOTO protocol enhanced staining of whole-mount plant tissues

In plants, some of the primary challenges when applying vEM is related to the cell walls, large air voids and water filled vacuoles which impede not only fixation and staining, but also impair overall sample conductivity, resulting in sensitivity to beam damage and charging artifacts. These difficulties are further exacerbated when working with cryo-fixation and freeze-substitution protocols, as organic solvent-based metal staining can be relatively limited due to low solubility, reduced chemical reactivity and overall poor staining of certain cell membranes (i.e., endoplasmic reticulum, nuclear envelope, mitochondria and thylakoids). Recent work applying vEM to freeze-substituted
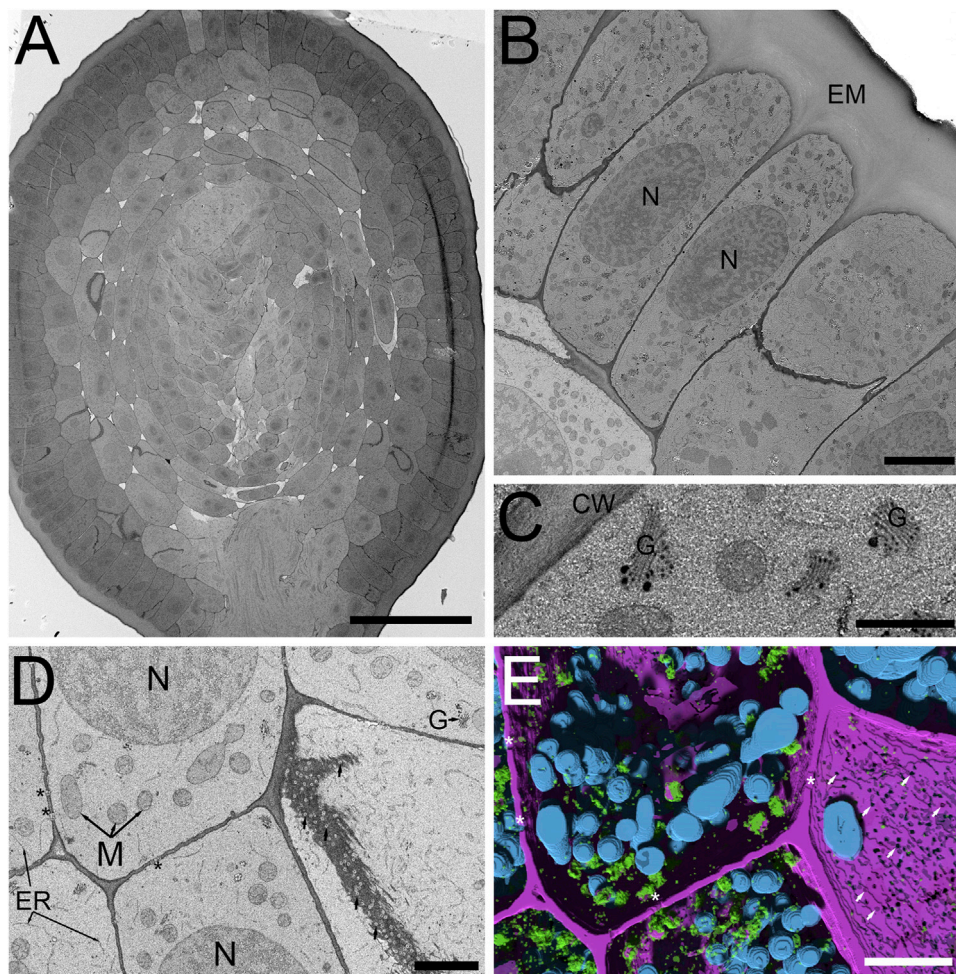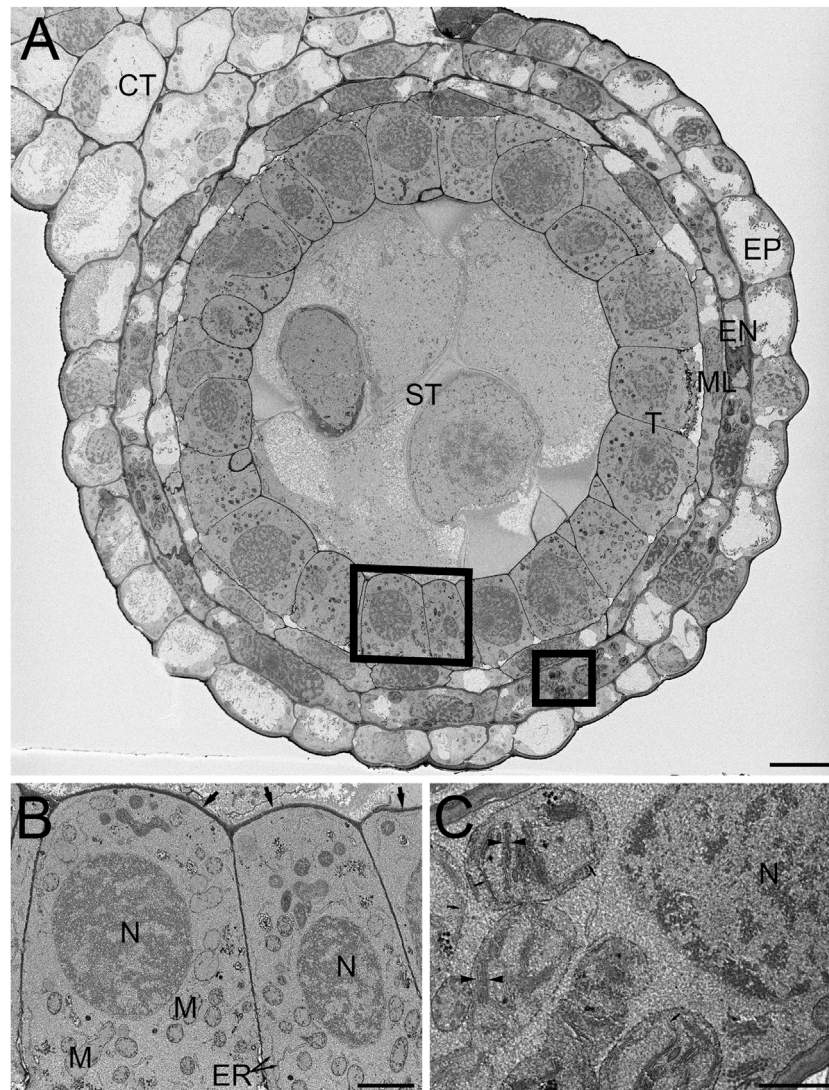
FIGURE 2
SBF-SEM of high-pressure frozen *H. vulgare* root prepared by FSaqOTO. **(A)**. SBF-SEM overview of root cross-section near the root apical meristem prepared by FSaqOTO. Scale = 100 μm. **(B)**. High-resolution SBF-SEM slice from **(A)** showing the outermost protoderm cells with nuclei (N), a normal array of other organelles and covered by a thin electron dense cell wall with a thick extracellular matrix (EM) on the root exterior. Scale = 5 μm. **(C)**. High magnification of a protoderm cell with well-stained Golgi membranes, cell wall and trans-Golgi vesicle contents. Scale = 0.5 μm. **(D)**. Rapidly dividing cells in the ground meristem exhibited well contrasted cell walls (CW) Golgi/vesicles (G) with clearly delineated nuclei (N), mitochondria (M) and electron transparent plasmodesmata (arrows). Scale = 1 μm. **(E)**. 3D rendering of **(D)** using Sensor 3D deep learning segmentation for mitochondria (cyan), Golgi and secretory vesicles (green) and cell wall (magenta) as well as intersecting plasmodesmata voids (asterisks). Scale = 1 μm.

anthers with organic solvent based OTO *en bloc* staining in combination with SBF-SEM and FCC, did improve accessibility for many biological questions in these important plant structures in our hands (Duncan et al., 2022). Despite considerable effort, we were unable to realize the full contrast benefits observed in traditional conventionally fixed specimens using aqueous-based OTO protocols while maintaining a strictly organic solvent-based processing routine after cryo-fixation. However, based on our recent success using conventional fixation with tobacco leaf tissues, the Hua protocol (Hua et al., 2015) was shown to be highly suitable for vEM and X-Ray microscopy. Thus, we reasoned that a modification of our freeze-substitution

protocol with a graded transition from an organic solvent-based (in our case acetone) 1% OsO_4 solution (containing water), to full rehydration in 1% OsO_4 aqueous buffer, followed by the Hua heavy metal staining steps, would enhance staining of freeze-substituted plant samples. Indeed, this concept worked with good effect in barley roots (Figure 2) and anthers (Figure 3) with SBF-SEM and FCC. A low magnification cross-section of a HPF FSaqOTO prepared barely root near the meristem (Figure 2A) showed high-density ground cytoplasmic matrix of the epidermal and cortex cells and elevated staining and electron density of the plant cell walls and vacuolar compartments (Figures 2B–D), Golgi apparatus and trans Golgi secretory
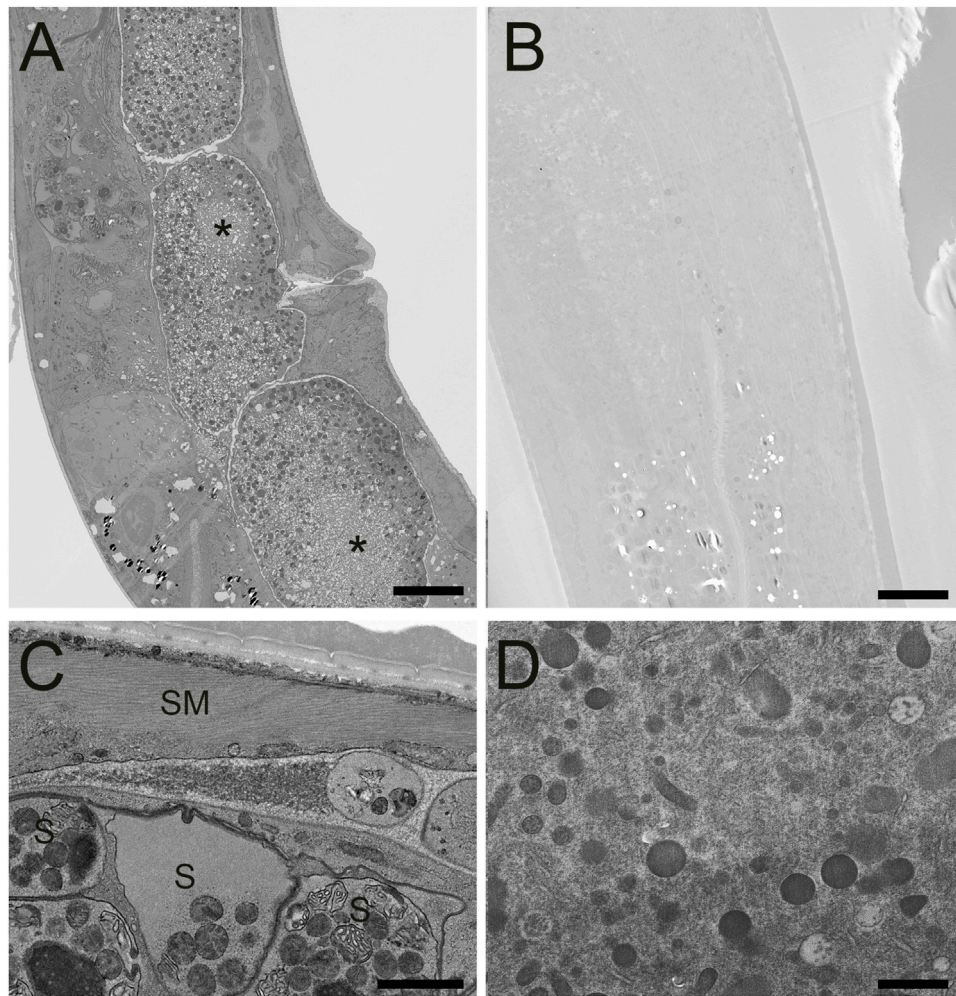
FIGURE 3
SBF-SEM of high-pressure frozen *H. vulgare* anther prepared by FSaqOTO. **(A)**. SBF-SEM overview of anther cross-section showing epidermal (EP), endothecium (EN), middle layer (ML), tapetum (T), sporogenous (ST) and connective tissue (CT). Scale = 10 μm. **(B)**. High magnification slice from region **(A)** (left box) showing the tapetum cells with nuclei (N), mitochondria (M) endoplasmic reticulum (ER) and covered by a thin electron dense cell wall (arrows). Scale = 1 μm. **(C)**. High magnification from region **(A)** (right box) well-stained well-stained chloroplastic membranes (arrows) and grana stacking readily visible (arrowheads). Scale = 0.5 μm.

vesicles (Figure 2C). Additionally, the plasma membrane, mitochondrial membranes and endoplasmic reticulum, while not heavily stained compared to conventional fixation OTO protocols, were readily discerned (Figure 2D). Indeed, this aided the success of deep learning segmentation (Sensor 3D, ORS Dragonfly) for 3D renderings (Figure 2E) of mitochondria (blue), Golgi and secretory vesicles (green) and cell wall (magenta) as well as intersecting plasmodesmata voids (arrows). Interestingly, plasmodesmata, which normally are more electron dense relative to the cell wall via electron microscopy, had inverted contrast (appeared electron

transparent in a more electron dense cell wall) (Figure 2D, Supplementary Video S1).

We then evaluated the FSaqOTO protocol for SBF-SEM and FCC on barley anthers, the male reproductive structure responsible for pollen production in plants. A low magnification overview of a single barley anther lobe allowed a clear assessment of the epidermal (EP), endothecium (EN), middle layer (ML), tapetum (T), sporogenous (ST) and connective tissue (CT) (Figure 3A). Similar to root tissues (Figure 2), the FSaqOTO showed elevated electron density in cells with high cytoplasmic density (Figures 3A–C) and highly

FIGURE 4
STEM of high-pressure frozen *C. elegans* prepared by FSaqOTO and traditional AFS. **(A)**. Low resolution overview longitudinal section of the nematode demonstrated very high contrast staining using FAaqOTO and using identical imaging conditions for **(B)** compared to a traditional AFS staining protocol. Local freeze-damage (asterisk). A and B, scale = 10 µm. **(C)**. FSaqOTO prepped sample at increased magnification with smooth muscle fibers (SM) clearly delineated, and well-stained membranes of spermatheeal (S), including the plasma membrane, mitochondria, other membranous organelles. Scale = 1 µm. **(D)**. Corresponding high magnification (compare to **4C**) with identical acquisition conditions of an AFS processed *C. elegans* but with a rescaled histogram demonstrated the normal complement of organelles but with notably relatively much reduced contrast, especially most cell membranes. Scale = 1 µm.

contrasted cell walls. Closer inspection of the tapetum (Figure 3B) revealed good contrast and discrimination of mitochondrial membranes, Golgi apparatus, endoplasmic reticulum and cell wall. While the nuclear envelope was visible, the elevated staining of the heterochromatin and nucleoplasm relative to the nuclear envelope, made it less conspicuous, especially in oblique profiles (Figures 2D),3B,C. In the endothecium, chloroplast thylakoid and grana membranes were readily contrasted and resolved (Figure 3C). Interestingly, in both plant tissues, non-membranous components of the cytoplasm, chloroplast stroma and nucleoplasm appeared to have a granular or textured appearance. In both tissue types,

over 1000 consecutive 10,000 × 10,000 pixel serial images were readily obtained at 5 nm x-y pixel resolution and 50 nm z-slice interval.

FSaqOTO protocol enhanced staining of whole-mount *C. elegans*

After verifying improved conductivity and overall elevated staining characteristics of our FSaqOTO protocol using SBF-SEM on challenging plant tissues, we tested if the method also provided similar improved staining with other
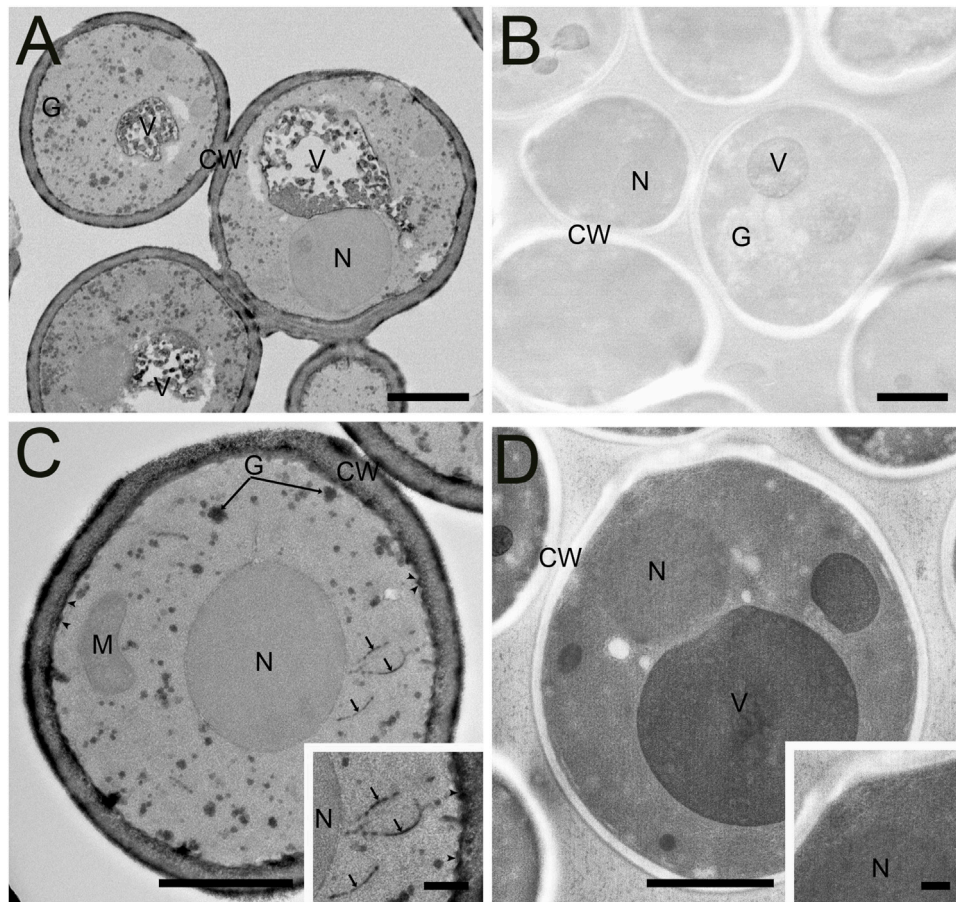
FIGURE 5
Comparison of high-pressure frozen yeast *S. cerevisiae* prepared by FSaqOTO and traditional AFS protocols and imaged via STEM and TEM. **(A)**. Overview STEM image of *S. cerevisiae* demonstrated very high contrast staining of the cell wall (CW), vacuolar contents (V) and their delimiting membrane and glycogen (G) using FAaqOTO and using identical imaging condition for **(B)** compared to a traditional AFS staining protocol. **(C)** and inset. FSaqOTO prepped yeast sample at increased magnification with well-labeled cell walls (CW), glycogen (G), plasmamembrane (arrowheads) cisternae (arrows), and elevated nuclear (N) and mitochondria (M) staining compared to AFS (5D) revealed. Scale = 1 µm. **(D)** and inset. Corresponding high magnification (compare to **5C**) with identical acquisition conditions of an AFS processed yeast but with a rescaled histogram demonstrated the normal complement of organelles but with much reduced contrast, especially cell membranes. **(A-D)** Scale = 1 µm, **(C)** and **(D)** insets = 100 nm.

phylogenetically distinct organisms. Furthermore, we wanted to compare the relative increase and differences in staining of cell structures when a quick freeze-substitution (QFS) protocol was used versus a traditional AFS freeze-substitution protocol. QFS is an excellent option for freeze-substitution in the absence of expensive instrumentation, with the added advantage of speed compared to AFS or freezer-based FS methods. For this work, we chose the model organisms *C. elegans* and *S. cerevisiae*; both represented challenging tests for EM staining protocols on account of their cuticle and cell wall, respectively, and were likely to show significant differences in staining with increased metallization, including vEM. For *C. elegans*, we noted a substantial contrast improvement across the organism when side-by-side AFS versus FSaqOTO

comparisons of worm longitudinal sections were made under identical image acquisition conditions (Figures 4A,B). We observed some freezing artifacts of the embryos (Figure 4A asterisk), which is unsurprising given the large size of the intact worm and chitinaceous shell of the embryo. It is likely that freezing was slowest at these depths, significantly away from the freezing surfaces during the HPF step. Nevertheless, at increased magnification, FSaqOTO of *C. elegans* demonstrated high contrast of various tissue and cell features. The fibers of smooth muscle were clearly delineated, and membranes of spermatheca, including the plasma membrane, mitochondria, and membranous organelles were well stained (Figure 4C). Similar to plant tissues, these samples had a textured cytoplasm and nucleoplasm. Under matched

image acquisition conditions (e.g. Figures 4C,D), but rescaled display histogram (Figure 4D only), the traditional AFS protocol lacked strong cytoplasmic and membrane staining, especially for the mitochondria and endoplasmic reticulum.

Like *C. elegans*, a direct comparison of traditional AFS and FSaqOTO protocols with the yeast, *S. cerevisiae*, evaluated by TEM demonstrated a substantial improvement in staining and contrast for FSaqOTO (Figures 5A,B) under identical acquisition and image display conditions. Of note is the strong contrast of the yeast cell wall, glycogen, plasma membrane, cisternae (Golgi equivalent) and vacuolar membrane and its contents (Figures 5A,C) compared to its AFS counterpart (Figures 5B,D). As with plant roots, anthers, and nematode samples, the ground cytoplasmic and nucleoplasm matrices exhibited a textured or slightly granular appearance (Figure 5C). While mitochondria and nuclei staining were notably elevated and visible in FSaqOTO (Figure 5C and inset) versus traditional AFS prepared *S. cerevisiae*, its mitochondrial membranes, nuclear envelope, and endoplasmic reticulum were essentially lacking in the AFS protocol, even after histogram rescaling the identically acquired image (Figure 5D and inset). FIB-SEM serial-sections of the FSaqOTO sample blocks were consistent with TEM data in contrasted structures (Supplementary Video S2).

Discussion

Over the last decade, a number of studies have applied the benefits of improved structural preservation, realized by combining cryo-preservation and freeze-substitution with vEM techniques, including yeast (Wei et al., 2012), nematode (Hall, Hartwieg and Nguyen, 2013; Rahman et al., 2021), plants (Czymmek et al., 2020; Reagan and Burch-Smith, 2022), fruit fly and mouse brain (Tsang et al., 2018), to name just a few. Continued improvements, such as by Guo et al. (2020), applied an organic solvent-based freeze-substitution protocol with a cocktail of OsO_4, tannic acid, uranyl acetate and potassium permanganate (without water) for improved membrane contrast and conductivity with FIB-SEM in a broad array of specimens (mouse brain, plants, algae, yeast and nematodes). Notably, earlier investigations with freeze-substitution with TEM in yeast demonstrated the benefits of adding very small amounts of water to the substitution fluid (1–5%) to specifically enhance the visibility of some cell membranes that were otherwise poorly contrasted (Buser and Walther, 2008). Other studies also showed the benefits of water in the initial freeze-substitution fluid for preserving fluorescent protein signals (and other fluorophores) within acrylic resin blocks for both vEM, lending such samples to more efficient correlative microscopy workflows (Peddie et al., 2014). Furthermore, organic solvent freeze-substitution protocols (with water) followed by the transition to an aqueous buffer and Tokuyasu cryo-sectioning (Ripper,

Schwarz and Stierhof, 2008) demonstrated notably improved antigenicity and morphology for several difficult plant, nematode, and fruit fly specimens using the Tokuyasu protocol. A related strategy to combine the benefits of freeze-substitution followed by rehydration with correlative workflows, termed "CryoChem" was recently developed (Tsang et al., 2018). This versatile approach used 0.2% glutaraldehyde plus 5% water in acetone before transitioning to buffer before further processing for fluorescence microscopy (fluorescent protein or DRAQ5), diaminobenzidine (DAB) reaction for APEX2 labeling (Lam et al., 2015; Martell et al., 2017) followed by OTO-based heavy metalization, resin infiltration before X-ray microscopy and/or FIB-SEM.

Our vEM FSaqOTO protocol was differentiated from the other freeze-substitution aqueous rehydration protocols, as we did not have a requirement for non-osmicated tissues to initially preserve fluorescence or other chemistries. As such, we were able to obtain the full benefits of a strong initial fixation with 2% OsO_4 (e.g., potentially reduced extraction) and a simplified protocol. Also of note, structures that are carbohydrate dense usually have very limited osmication and metal staining in standard EM protocols. However, in our work, we found that the addition of potassium ferrocyanide, followed by the direct exchange into OsO_4 (without rinsing) per Hua (Hua et al., 2015), consistently provided very strong contrast of certain carbohydrate dense plant cell walls, yeast cell walls, the lumen of Golgi and secretory vesicles and glycogen (Figures 2B–D; Figures 3A,B; Figures 5A,C). This observation is consistent with the well-known properties of some potassium salts (e.g., potassium permanganate and potassium ferrocyanide) to enhance glycogen contrast in conventional fixation preparations (Revel et al., 1960; Goldfischer et al., 1981). Not surprisingly, for plants, algae and yeast, when potassium permanganate was included in the freeze-substitution fluid of the FIBSEM protocol used by Guo (Guo et al., 2020), a similar increased labeling of cell walls in these organisms and glycogen in yeast was observed.

As mentioned previously, the addition of a small percentage of water to substitution fluid improves certain organelle membrane visibility in freeze-substitution (Buser and Walther, 2008). This is especially evident when we compare chloroplastic, thylakoid and grana membranes, which normally lack significant contrast in non-aqueous freeze-substitution preparations (Bourett et al., 1999; Bobik, Dunlap and Burch-Smith, 2014; Czymmek et al., 2020) but are very conspicuous in most conventional fixation (Kaneko and Walther, 1995; McDonald, 2014; Anderson et al., 2021). While the addition of water alone to the substitution will have some benefit, we observed that in combination with our FSaqOTO approach that chloroplast membranes were very prominent (Figure 3C) with easy visualization of individual stacks of grana membrane and lumen via vEM will open doors to improved resolution, 3D visualization and quantification of these cryo-preserved structures in bulk samples. Furthermore, while not nearly as prominent an improvement as membranes in conventional

fixation OTO methods, overall, our protocol did appear to enhance all cytoplasmic structures including cellular membranes of *C. elegans* and *S. cerevisiae* over our traditional AFS (compare Figures 4A,C with Figures 4B,D; Figures 5A,C with Figures 5B,D). Indeed, much groundwork has been laid in the field for vEM of both *S. cerevisiae* (Winey et al., 1995; Buser and Walther, 2008; Wei et al., 2012; Wu et al., 2020) and *C. elegans* (Hall et al., 2013; Rahman et al., 2020, 2021) with cryo-preservation and freeze-substitution. Specifically, our traditional AFS protocol used here was very similar to substitution chemistry with prior Narayan lab work in *C. elegans*. However, here, virtually all structures (membrane or not) had elevated staining beyond our other standard method (Compare Figures 4A,C with Figures 4B,D, Figures 5A,C with Figures 5B,D) which benefited overall sample signal, contrast, and conductivity for vEM. We wanted to directly compare our FSaqOTO and traditional freeze-substitution AFS protocols using identical image acquisition and display conditions (Compare 4A with 4B, 5A with 5B) via STEM and TEM. Our comparison was specifically optimized for our FSaqOTO samples and then we reproduced the same imaging conditions for the AFS processed samples. We note that for both our *C. elegans* and *S. cerevisiae* specimens, the beam conditions to acquire a high quality FSaqOTO image were inadequate for the AFS processed samples. While it is true that our acquisition conditions could be further optimized for our AFS prepared samples, our comparison sought to allow a side-by-side appreciation of the substantial sample staining improvement using the high-contrast FSaqOTO samples as the baseline. Furthermore, at higher magnification, the freeze-substitution staining of sensitive membrane structures (e.g., thylakoid, endoplasmic reticulum, nuclear envelope) could not be appreciably recovered in either AFS specimen (Compare Figure 4C with Figures 4D, Figure 5C with Figure 5D), even with optimized imaging conditions. The metallization staining gains allowed in our tested samples also enabled the samples to tolerate increased beam dosage without noticeable beam damage artifacts. Indeed, elevation of the sample stain allowed enhanced conductivity, increased and more signal from selected sample features, which resulted in improved overall signal-to-noise and resolution. To appreciate this, comparison with previous work using a polar solvent-based OTO freeze-substitution protocol on *Arabidopsis thaliana* anthers (Czymmek et al., 2020) and using the same SBF-SEM system with FCC, reflected the electron dosage this sample could tolerate (accelerating voltage 2.5 kV, beam current 1 pA, dwell-time 0.8 μs, z-slice 70 nm, pixel size 5 nm pixels). While for the *H. vulgare* anthers analyzed here, we used the same pixel size (5 nm) and probe current (1 pA), but were able to double the accelerating voltage to 5 kV with a 3.75-fold greater dwell-time (3 μs/pixel) as well as reliably cutting at a thinner z-slice of 50 nm (Figures 2, 3, Supplementary Video S1). Likewise, our FSaqOTO prepared yeast 3D FIB-SEM volumes (Supplementary Video S2) versus our previous work using traditional freeze-

substitution via FIB-SEM (Wei et al., 2012) had nearly identical beam acquisition conditions for our FSaqOTO samples (accelerating voltage 1.5 keV, probe current ~1 nA). However, at 381 μsec/pixel average total dwell-time/image calculated from the earlier work versus FSaqOTO at 3 μsec/pixel average total dwell-time/image reflects over a 100-fold reduction in average pixel dwell-time/image. Thus, in both the anther and yeast instances, much improved throughput and/or signal-to-noise and could allow significant gains for many other types of similarly cryo-prepared vEM samples.

Not unlike the morphological differences in staining selectivity between conventional fixation OTO versus traditional non-OTO EM protocols, our FSaqOTO protocol had a different appearance and staining pattern when compared to traditional freeze-substitution. Notably, while the overall organelle/membrane enhancement appeared to be improved, the selectivity was less prominent compared to conventional fixation OTO protocols. Strictly aqueous-based conventional fixation OTO protocols have remarkably enhanced membrane contrast (Deerinck et al., 2018; Lippens et al., 2019). While FSaqOTO had a different appearance from other standard freeze-substitution protocols, it was characterized by consistently elevated tissue staining in all tested samples and fixation conditions. Furthermore, we noted that the cytoplasm and nucleoplasm of all cell types exhibited a granular/textured appearance that may reflect some level of nano-aggregation artifact of unknown origin. While this granular phenomenon may in part aid in the improved overall sample metallization and conductivity, it brings attention to the limits of the approach for certain questions that require high-fidelity, high-resolution ultrastructural studies.

Overall, our improved FSaqOTO method allowed more reliable vEM data acquisition and extended the experimental possibilities for cryo-preserved samples that are otherwise limited by low contrast and low conductivity organic solvent-based staining protocols. The addition of water in the substitution fluid and a straightforward solvent to water transition for heavy metal staining enabled noteworthy improvement in contrast with many structures. Furthermore, these samples realized a much-improved sample tolerance to electron beam dosage which enabled longer integration times and increased resolution resulting in better signal-to-noise for a given pixel size. Alternatively, the approach can allow increased throughput for freeze-substituted vEM studies enabling more samples or larger volumes imaged per unit time. Finally, there are numerous opportunities for the modification and/or improvement of our staining strategy via adjustments to the substitution fluid (Ripper et al., 2008; Guo et al., 2020), aqueous OTO and metalization steps (Deerinck et al., 2018; Genoud et al., 2018) and/or combination with correlative approaches (Caplan et al., 2011; Tsang et al., 2018; Duncan et al., 2022). Ultimately, we hope that our modified freeze-substitution vEM staining strategy will stimulate more labs to explore other recipes for improved selection and enhancement of target cell structures while

maintaining the full benefits of cryo-preservation and freeze-substitution.

Data availability statement

The raw data supporting the conclusions of this article will be made available by the authors, without undue reservation.

Author contributions

KC conceived of approach, SB, HB, VB, KC, KD, and KN performed sample preparation and/or imaging. KC and KN wrote and edited manuscript. SB, KD, and BM edited manuscript.

Acknowledgments

Conflict of interest

The authors declare that the research was conducted in the absence of any commercial or financial relationships that could be construed as a potential conflict of interest.

Publisher's note

All claims expressed in this article are solely those of the authors and do not necessarily represent those of their affiliated organizations, or those of the publisher, the editors and the reviewers. Any product that may be evaluated in this article, or claim that may be made by its manufacturer, is not guaranteed or endorsed by the publisher.

Supplementary material

The Supplementary Material for this article can be found online at: https://www.frontiersin.org/articles/10.3389/fcell.2022.933376/full#supplementary-material

References

Anderson, C. M., Mattoon, E. M., Zhang, N., Becker, E., McHargue, W., Yang, J., et al. (2021). High light and temperature reduce photosynthetic efficiency through different mechanisms in the C4 model Setaria viridis. *Commun. Biol.* 4 (1), 1092. doi:10.1038/s42003-021-02576-2

Bobik, K., Dunlap, J. R., and Burch-Smith, T. M. (2014). Tandem high-pressure freezing and quick freeze substitution of plant tissues for transmission electron microscopy. *J. Vis. Exp.* (92), e51844. doi:10.3791/51844

Bourett, T. M., Czymmek, K. J., and Howard, R. J. (1999). Ultrastructure of chloroplast protuberances in rice leaves preserved by high-pressure freezing. *Planta* 208 (4), 472–479. doi:10.1007/s004250050584

Buser, C., and Walther, P. (2008). Freeze-substitution: The addition of water to polar solvents enhances the retention of structure and acts at temperatures around -60 degrees C. *J. Microsc.* 230 (2), 268–277. doi:10.1111/j.1365-2818.2008.01984.x

Caplan, J., Niethammer, M., Taylor, R. M., and Czymmek, K. J. (2011). The power of correlative microscopy: Multi-modal, multi-scale, multi-dimensional. *Curr. Opin. Struct. Biol.* 21 (5), 686–693. doi:10.1016/j.sbi.2011.06.010

Collman, F., Buchanan, J., Phend, K. D., Micheva, K. D., Weinberg, R. J., and Smith, S. J. (2015). Mapping synapses by conjugate light-electron array tomography. *J. Neurosci.* 35 (14), 5792–5807. doi:10.1523/JNEUROSCI.4274-14.2015

Czymmek, K., Sawant, A., Goodman, K., Pennington, J., Pedersen, P., Hoon, M., et al. (2020). "Imaging plant cells by high-pressure freezing and serial block-face scanning electron microscopy," in *Springer protocols, plant Endosomes*. Editor M. S. Ortegui (Springer US), 69–81. doi:10.1007/978-1-0716-0767-1_7

Deerinck, T. J., Shone, T. M., Bushong, E. A., RamachandRa, R., Peltier, S. T., and Ellisman, M. H. (2018). High-performance serial block-face SEM of nonconductive biological samples enabled by focal gas injection-based charge compensation. *J. Microsc.* 270 (2), 142–149. doi:10.1111/jmi.12667

Denk, W., and Horstmann, H. (2004). Serial block-face scanning electron microscopy to reconstruct three-dimensional tissue nanostructure. *PLoS Biol.* 2 (11), e329. doi:10.1371/journal.pbio.0020329

Duncan, K. E., Czymmek, K. J., Jiang, N., Thies, A. C., and Topp, C. N. (2022). X-ray microscopy enables multiscale high-resolution 3D imaging of plant cells, tissues, and organs. *Plant Physiol.* 188 (2), 831–845. doi:10.1093/plphys/kiab405

Genoud, C., Titze, B., Graff-Meyer, A., and Friedrich, R. W. (2018). Fast homogeneous *en bloc* staining of large tissue samples for volume electron microscopy. *Front. Neuroanat.* 12, 76. doi:10.3389/fnana.2018.00076

Gilkey, J. C., and Staehelin, L. A. (1986). Advances in ultrarapid freezing for the preservation of cellular ultrastructure. *J. Electron Microsc. Tech.* 3 (2), 177–210. doi:10.1002/jemt.1060030206

Goldfischer, S., Kress, Y., Coltoff-Schiller, B., and Berman, J. (1981). Primary fixation in osmium-potassium ferrocyanide: The staining of glycogen, glycoproteins, elastin, an intranuclear reticular structure, and intercisternal trabeculae. *J. Histochem. Cytochem.* 29 (9), 1105–1111. doi:10.1177/29.9.6169760

Guérin, C. J., Kremer, A., Borghgraef, P., and Lippens, S. (2019). Targeted studies using serial block face and focused ion beam scan electron microscopy. *J. Vis. Exp.* (150). doi:10.3791/59480

Guo, J., Wang, G., Tang, W., Song, D., Wang, X., Hong, J., et al. (2020). An optimized approach using cryofixation for high-resolution 3D analysis by FIB-SEM. *J. Struct. Biol.* 212 (1), 107600. doi:10.1016/j.jsb.2020.107600

Hall, D. H., Hartwieg, E., and Nguyen, K. (2013). *WormAtlas anatomical methods - OTO fixation for SEM blockface imaging*. WormAtlas: L. A. Herndon. doi:10.3908/wormatlas.9.8

Hoffman, D. P., Shtengel, G., Xu, C. S., Campbell, K. R., Freeman, M., Wang, L., et al. (2020). Correlative three-dimensional super-resolution and block-face electron microscopy of whole vitreously frozen cells. *Science*, 367 (6475), eaaz5357. doi:10.1126/science.aaz5357

Hua, Y., Laserstein, P., and Helmstaedter, M. (2015). Large-volume *en-bloc* staining for electron microscopy-based connectomics. *Nat. Commun.*, 6, 1–7. doi:10.1038/ncomms8923

Kaneko, Y., and Walther, P. (1995). Comparison of ultrastructure of germinating pea leaves prepared by high-pressure freezing-freeze substitution and conventional chemical fixation. *J. Electron Microsc.* 44 (2), 104–109. doi:10.1093/oxfordjournals.jmicro.a051149

Lam, S. S., Martell, J. D., Kamer, K. J., Deerinck, T. J., Ellisman, M. H., Mootha, V. K., et al. (2015). Directed evolution of APEX2 for electron microscopy and proximity labeling. *Nat. Methods* 12 (1), 51–54. doi:10.1038/nmeth.3179

Lippens, S., Kremer, A., Borghgraef, P., and Guérina, C. J. (2019). Serial block face-scanning electron microscopy for volume electron microscopy. *Methods Cell Biology,Three-Dimensional Electron Microsc.*, 69–85. doi:10.1016/bs.mcb.2019.04.002

Mahamid, J., et al. (2015). A focused ion beam milling and lift-out approach for site-specific preparation of frozen-hydrated lamellas from multicellular organisms. *J. Struct. Biol.*, 192. Elsevier, 262–269. doi:10.1016/j.jsb.2015.07.012

Martell, J. D., Deerinck, T. J., Lam, S. S., Ellisman, M. H., and Ting, A. Y. (2017). Electron microscopy using the genetically encoded APEX2 tag in cultured mammalian cells. *Nat. Protoc.* 12 (9), 1792–1816. doi:10.1038/nprot.2017.065

McDonald, K. L. (2014). Out with the old and in with the new: Rapid specimen preparation procedures for electron microscopy of sectioned biological material. *Protoplasma* 251 (2), 429–448. doi:10.1007/s00709-013-0575-y

Mcdonald, K. L., and Webb, R. I. (2011). Freeze substitution in 3 hours or less. *J. Microsc.* 243 (3), 227–233. doi:10.1111/j.1365-2818.2011.03526.x

Mendenhall, J. M., Kuwajima, M., and Harris, K. M. (2017). Automated serial section large-field transmission-mode scanning electron microscopy (tSEM) for volume Analysis of Hippocampus ultrastructure. *Microsc. Microanal.* 23 (S1), 562–563. doi:10.1017/S143192761700349X

Narayan, K., Danielson, C. M., Lagarec, K., Lowekamp, B. C., Coffman, P., Laquerre, A., et al. (2014). Multi-resolution correlative focused ion beam scanning electron microscopy: Applications to cell biology. *J. Struct. Biol.*, 185. Elsevier, 278–284. doi:10.1016/j.jsb.2013.11.008

Narayan, K., and Subramaniam, S. (2015). Focused ion beams in biology. *Nat. Methods*, 12, 1021–1031. doi:10.1038/nmeth.3623

Nguyen, H. B., Thai, T. Q., Saitoh, S., Wu, B., Saitoh, Y., Shimo, S., et al. (2016). Conductive resins improve charging and resolution of acquired images in electron microscopic volume imaging. *Sci. Rep.* 6, 1–10. doi:10.1038/srep23721

Otegui, M. S. (2020) 'Electron tomography and immunogold labeling of plant cells'. *Methods Cell Biology,Plant Cell Biol.* 21–36. doi:10.1016/bs.mcb.2020.06.005

Peddie, C. J., Blight, K., Wilson, E., Melia, C., Marrison, J., Carzaniga, R., et al. (2014). Correlative and integrated light and electron microscopy of in-resin GFP fluorescence, used to localise diacylglycerol in mammalian cells. *Ultramicroscopy* 143 (100), 3–14. doi:10.1016/j.ultramic.2014.02.001

Rahman, M., Chang, I. Y., Cohen-Fix, O., and Narayan, K. (2021). A workflow for high-pressure freezing and freeze substitution of the *Caenorhabditis elegans* embryo for ultrastructural analysis by conventional and volume electron microscopy. *Bio. Protoc.* 11 (7), e3981. doi:10.21769/BioProtoc.3981

Rahman, M., Chang, I. Y., Harned, A., Maheshwari, R., Amoateng, K., Narayan, K., et al. (2020). C. elegans pronuclei fuse after fertilization through a novel membrane structure. *J. Cell Biol.* 219 (2), e201909137. doi:10.1083/jcb.201909137

Reagan, B. B., and Burch-Smith, T. M. (2022). "Focused ion beam-scanning electron microscopy for investigating plasmodesmal densities," in *Plasmodesmata: Methods and protocols*. Editors M.Y. HeinleinBenitez-Alfonso. 978-1-0716-2131-8.

Revel, J. P., Napolitano, L., and Fawcett, D. W. (1960). Identification of glycogen in electron micrographs of thin tissue sections. *J. Biophys. Biochem. Cytol.* 8 (3), 575–589. doi:10.1083/jcb.8.3.575

Ripper, D., Schwarz, H., and Stierhof, Y.-D. (2008). Cryo-section immunolabelling of difficult to preserve specimens: Advantages of cryofixation, freeze-substitution and rehydration. *Biol. Cell* 100 (2), 109–123. doi:10.1042/bc20070106

Smith, S. J. (2018). Q& a: Array tomography', *BMC biology*. *BMC Biol.* 16 (1), 98. doi:10.1186/s12915-018-0560-1

Sydor, A. M., Czymmek, K. J., Puchner, E. M., and Mennella, V. (2015). Super-resolution microscopy: From single molecules to supramolecular assemblies. *Trends Cell Biol.* 25 (12), 730–748. doi:10.1016/j.tcb.2015.10.004

Titze, B., and Genoud, C. (2016). Volume scanning electron microscopy for imaging biological ultrastructure. *Biol. Cell* 108 (11), 307–323. doi:10.1111/boc.201600024

Tsang, T. K., Bushong, E. A., Boassa, D., Hu, J., Romoli, B., Phan, S., et al. (2018). High-quality ultrastructural preservation using cryofixation for 3d electron microscopy of genetically labeled tissues. *eLife* 7, e35524. doi:10.7554/eLife.35524

Watanabe, S., Lehmann, M., Hujber, E., Fetter, R. D., Richards, J., Sohl-Kielczynski, B., et al. (2014). Nanometer-resolution fluorescence electron microscopy (nano-EM) in cultured cells. *Methods Mol. Biol.* 1117, 503–526. doi:10.1007/978-1-62703-776-1_22

Wei, D., Jacobs, S., Modla, S., Zhang, S., Young, C. L., Cirino, R., et al. (2012). High-resolution three-dimensional reconstruction of a whole yeast cell using focused-ion beam scanning electron microscopy. *BioTechniques* 53 (1), 41–48. doi:10.2144/000113850

Winey, M., Mamay, C. L., O'Toole, E. T., Mastronarde, D. N., Giddings, T. H., McDonald, K. L., et al. (1995). Three-dimensional ultrastructural analysis of the *Saccharomyces cerevisiae* mitotic spindle. *J. Cell Biol.* 129 (6), 1601–1615. doi:10.1083/jcb.129.6.1601

Wu, G.-H., Mitchell, P. G., Galaz-Montoya, J. G., Hecksel, C. W., Sontag, E. M., Gangadharan, V., et al. (2020). Multi-scale 3D cryo-correlative microscopy for vitrified cells. *Structure* 28, 1231–1237. doi:10.1016/j.str.2020.07.017